1990 SCA CONFERENCE PAPER #9011

ADVANCES IN CENTRIFUGE METHODOLOGY FOR CORE ANALYSIS

M. J. King
K. R. Narayanan
A. J. Falzone

BP RESEARCH
BP America, Inc.
4440 Warrensville Center Road
Cleveland, Ohio 44128-2837

ABSTRACT

The centrifuge provides a powerful tool for the determination of relative permeability, capillary pressure, and residual saturation. Experiments may be performed rapidly, and over a wide range of accelerations, to effectively displace fluid from core samples. Advances in instrumentation have provided information on fluid production, with high volumetric and temporal accuracy. Advances in analysis utilize semi-analytic and numerical techniques to obtain detailed information on displacement mechanisms. Experimental results are presented for Berea sandstone, and for reservoir rock samples, emphasizing the transient production of oil in a gravity drainage process.

A critical review is provided of the usual methods of centrifuge methodology for core analysis. Lack of mechanical equilibrium, and the stripping of non-wetting phase residual (Critical Bond number effects) may compromise the determination of capillary pressure. Finite core length effects will be described as well. The usual analysis of transient production for relative permeability neglects the effects of capillary retention of fluid. This will bias the resulting relative permeability, leading to artificially high values of residual saturation.

History matching can provide the correction of capillary pressure for lack of equilibrium, and the correction of relative permeability as capillary retention becomes important. However, the results may be dependent upon the models of relative permeability and capillary pressure which are introduced. It is shown how a combined analytical / numerical approach can provide unbiased estimates of these curves. Recommended core analysis methodologies, both experimental and analytic, are provided.

INTRODUCTION

The centrifuge has proven to be a valuable tool for measuring capillary pressure [1-10] and relative permeabilities [13-15] of small core samples. Other techniques have been proposed for measuring capillary pressures [16-19]. These include the porous plate, mercury injection, and the water vapor desorption method. The porous plate technique is perhaps the most direct way to measure capillary pressure in a rock sample but this technique suffers from long equilibration times. The mercury injection technique, on the other hand is fairly rapid, but it is difficult to extrapolate the results from this method, which uses mercury and air as the nonwetting and wetting fluids respectively, to oil-water systems.

Relative permeability curves for a given rock sample may be measured from the steady-state or unsteady-state core displacement experiments. The steady-state method is a direct method for obtaining relative permeabilities from experimental data, but it is very tedious and time consuming. Unsteady-state experiments are rapid and relatively easy to perform. Explicit techniques such as the Johnson, Bossler and Naumann (JBN) technique [20], are used to calculate relative permeabilities from unsteady-state experiments. The JBN method makes several assumptions, especially that the flow be stable and uniform and that capillary effects can be ignored. Calculated results may be unreliable for displacements with adverse mobility ratio or for heterogeneous samples. Displacement experiments at low flow rates are more uniform, but may be dominated by capillary end effects. Analyses which attempt to correct for this [21,22] require knowledge of the capillary pressure curve.

Unlike unsteady-state core floods, displacements in the centrifuge do not suffer from viscous instabilities. Also, the method attains hydrostatic equilibrium faster than the porous plate method, and measurements can be extended to larger values of capillary pressure (lower relative permeability) than in core flood. As pointed out by Hagoort [23], the centrifuge method may be the most accurate and efficient method for studying the gravity drainage process in core samples. The low values of oil relative permeabilities determined by this method may be unattainable by other means. O'Meara and Crump [13], and more recently Nordvedt et.al. [15], used a numerical simulator to determine capillary pressure and relative permeability by history matching the production data from a centrifuge run performed at several speeds.

Jennings, McGregor and Morse [24] have demonstrated a rapid porous plate technique for measuring both capillary pressure and wetting phase relative permeability in a single experiment by using plastic semi-permeable membranes of a few microns thickness. The rapid porous plate technique, due to the low displacement pressures of reasonably permeable diaphragms, is limited to regions of low capillary pressures or regions of high saturations.

REVIEW OF CENTRIFUGE METHODOLOGY

The centrifuge has been applied to the determination of capillary pressure, and relative permeability, in both imbibition and drainage situations. For the purpose of this review, we shall

examine the determination of capillary pressure, providing a uniform presentation of the major analyses, dating back to Hassler and Brunner [1]. The exact solution to this problem will be provided; the literature will be reviewed in the context of this solution. The determination of relative permeability is a current research topic; it will be discussed in subsequent sections of this paper.

Hassler and Brunner (HB) provided a complete formulation of the capillary pressure problem. The notations and presentation will follow King [7], but will be generalized to include both imbibition and drainage. In particular we either consider the forced imbibition of water into an oil saturated rock, or the drainage of oil during a gas flood (gravity drainage). The initial oil saturation is in mechanical equilibrium when the centrifuge is not rotating, i.e., Pc = 0 when $\omega = 0$. The centrifuge is accelerated to some rotation rate, ω, and remains at that rotation rate until oil production ceases. In practice, equilibrium effects must be discussed, but for now will be ignored.

If r_a is the distance from the centrifuge rotation axis to the core outlet, and r_b to the inlet, then

$$P_c = \frac{1}{2} \Delta\rho \, (r_a^2 - r^2) \, \omega^2 \qquad (1)$$

gives the variation of capillary pressure through the core; $\Delta\rho$ is the (positive) fluid density difference ($\rho_{water}-\rho_{oil}$, or $\rho_{oil}-\rho_{gas}$). Fig.1 is a schematic of the drainage configuration. The analysis proceeds by relating the experimentally observed average saturation $\langle S \rangle(\omega^2)$ to the saturation at the inlet of the core. With the assumption of capillary equilibrium, the capillary pressure function (Pc(S), or equivalently $S[Pc(r,\omega^2)]$) can be used to relate the saturation at a point in the core to the saturation at the core inlet, r_b. Define,

$$S_b(\omega^2) = S[Pc(r_b, \omega^2)] \qquad (2)$$

Hence,

$$S[Pc(r, \omega^2)] = S_b(z \, \omega^2) \qquad (3)$$

where

$$z = Pc(r, \omega^2) \; / \; Pc(r_b, \omega^2) \qquad (4a)$$

$$= (r^2 - r_a^2) \; / \; (r_b^2 - r_a^2) \qquad (4b)$$

is the fractional capillary pressure through the core. Following [1,7] we can express the experimental mass balance as

$$\left(\frac{2 \, r_a}{r_a + r_b} \right) \cdot \langle S \rangle(\omega^2) = \int_0^1 dz \, (1 + \epsilon \, z)^{-1/2} \, S_b(z \, \omega^2) \qquad (5)$$

where ϵ

$$\epsilon = (r_b^2 - r_a^2) \; / \; r_a^2 \qquad (6)$$

is a small quantity dependent upon core length and rotor size. This is the fundamental equation first derived by HB. It is an integral equation which relates the unknown integrand to the experimental data. Through the core, the capillary pressure varies from zero at the outlet, to $Pc(r_b,\omega^2)$.

Following [1], define,

$$S_{HB}(\omega^2) = \frac{d}{d\omega^2}\left[\omega^2 \cdot \langle S\rangle(\omega^2)\right] \tag{7}$$

Operating on Eqn. (5), and integrating by parts, one obtains an integral equation for $S_b(\omega^2)$.

$$S_b(\omega^2) = A \cdot S_{HB}(\omega^2) - B \cdot \int_0^1 dz\, U(z) \cdot S_b(z\,\omega^2) \tag{8}$$

where A, B, and U(z) are defined by

$$A = \left(\frac{2r_b}{r_a + r_b}\right), \qquad B = \left(\frac{r_b^2 - r_a^2}{2\,r_b^2}\right) \tag{9a,b}$$

$$U(z) = z \cdot \left(\frac{1+\epsilon}{1+\epsilon\, z}\right)^{3/2} \tag{10}$$

Equation (8) can formally be solved by an appropriate Green's function.

$$S_b(\omega^2) = A \cdot \left\{ S_{HB}(\omega^2) - B \cdot \int_0^1 dz\, W(z) \cdot S_{HB}(z\,\omega^2) \right\} \tag{11}$$

where W(z) is related to U(z).

$$W(z) = U(z) - B \cdot \int_0^1 dx\, U(x) \int_0^1 dy\, W(y) \cdot \delta(x \cdot y - z) \tag{12}$$

The structure of Eqn. (11) also becomes apparent upon successive substitutions in Eqn. (8). Eqn. (12) is solvable by ordinary numerical methods, where the Dirac delta function is used to perform one of the pair on integrations. Unlike direct solutions of either Eqn. (5) or of Eqn. (8), there are no experimental saturations involved, and no need for data smoothing. We have utilized both finite difference and numerical Laplace transform solutions to Eqn. (12). The latter are performed by defining,

$$\tilde{f}(p) = \int_0^1 dz\, z^{p-1} f(z) \tag{13}$$

hence

$$\tilde{W}(p) = \tilde{U}(p) \,/\, (1 + B \cdot \tilde{U}(p)) \tag{14}$$

which can be inverted numerically.

Equation (11) forms the basis for a numerical algorithim, which is used routinely. More details of the algorithim are discussed in [7]. It is interesting to note that the algorithim can be split into two parts. In the first part the experimental saturation points are corrected for finite length

effects, i.e., they are modified to the values they would have had with a zero length core. This construction utilizes the W(z) function, and is independent of the capillary pressure curve. From Eqn. (11),

$$\langle S\rangle_0(\omega^2) = A \cdot \left\{ \langle S\rangle(\omega^2) - B \cdot \int_0^1 dz\, W(z) \cdot \langle S\rangle(z\,\omega^2) \right\} \quad (15)$$

and

$$S_b(\omega^2) = \frac{d}{d\omega^2}\left(\omega^2 \cdot \langle S\rangle_0(\omega^2) \right) \quad (16)$$

The second part of the algorithim, is provided by Eqn. (16). The Hassler-Brunner construction now provides an exact answer since $\langle S\rangle_0$ is the production from the equivalent zero length core.

Typical results are shown in Fig.3. Data was obtained from a 200 mDarcy Berea sample, with a value of ϵ = -0.50756. The negative sign arises in drainage experiments, consistent with the definition of ϵ. It is seen that there is only a small shift in the data, consistent with the HB approximation.

A literature survey is summarized in Table 1, starting with the current work, as a standard form. The 1948 HB approximation appears next. HB suggested that their solution could be used as the basis of a systematic perturbation expansion, and provided the limits on core length for which their approximation would hold. The first attempt to provide an extension to HB, was Hoffman [2]. As noted by Luffel [3], this derivation was incorrect. In the current language, the function W(z) is set to zero. In recent years there have been several more attempts. van Domselaar's construction [4] can be written in standard form with W(z) replaced by its average. This is most evident by following the exposition of Melrose [5]. This average may be integrated analytically, in the manner of Eqn. (14).

The most recent approximation is that of Rajan [6]. As noted by Ayappa [8], the result of Rajan may either be interpreted as an integral equation to be solved, or as an approximation. After extensive manipulation (not shown), the approximate Rajan solution can be manipulated into standard form, to define a function $\rho(z)$. Fig.4 provides examples of W(z) and $\rho(z)$, as well as the average of W, and the function U(z) used in the construction of W. It is interesting to note that the $\rho(z)$ function is quite close to U(z), indicating that Rajan's solution is a first order accurate approximation to W(z). It is expected that use of U(z) in place of $\rho(z)$ would provide answers to the same order of accuracy as Rajan's. In place of solving an integral equation for W(z), type curves have been provided in Fig.5 for a range of ϵ commonly encountered.

There are a number of aspects of centrifuge capillary pressure that are beyond the scope of this review. For example, finite core width effects have been discussed by Christiansen and Cerise [9]. Use has been made of parameter estimation to interpret the centrifuge [10] experiments. As discussed in more detail later, use of a restrictive functional form may provide highly biased answers.

One important additional aspect relates to the distinction between imbibition and drainage centrifugation. In the drainage process, we consider the eventual production of wetting phase by continuous thin film flow. The relative permeability is expected to be quite small, nonetheless, the

phase retains continuity and the phase pressure remains a valid concept. Not so in imbibition, where the non-wetting phase will become discontinuous and trapped. This has been experimentally observed by Wunderlich [11], and discussed by Melrose [5], and others [7]. Once discontinuity occurs, the entire capillary pressure analysis is invalid. The analysis may be replaced [7] by a mass balance construction based on the Bond number,

$$N_B = k \Delta\rho r \omega^2 / \sigma \qquad (17)$$

i.e., the ratio of buoyancy to surface forces. One finds that a plot of the experimental saturation against the logarithm of the mid-core Bond number gives an excellent approximation to a residual saturation curve, expressing capillary desaturation. The experimental signal for this discontinuity appears in a change of concavity on this plot. It should be noted that a parameter estimation technique which assumed a clean asymptote at residual oil saturation would be unable to detect this information.

Two criteria have been proposed to estimate when desaturation will occur. Melrose has provided an analysis based on the Leverett number, which provides a conservative bound to the desaturation observed in Wunderlich's experiments. A tighter bound is provided by the estimate of a critical Bond Number of 10^{-5}. The latter appears to hold for both Berea, and for reservoir samples, and is clearly related to the critical Capillary Number [12] observed in coreflood experiments.

EXPERIMENTAL DETAILS

High quality transient production data is obtained utilizing an automated ultracentrifuge. The apparatus is a Beckman ultracentrifuge in which the work of the operator has been automated. The control system is capable of operating the centrifuge, monitoring the rotor speed, operating the strobe and timing it to flash when a selected bucket is above the strobe, as well as acquiring, storing and analyzing the data.

Oil and water produced from the rock sample are collected in standard Beckman receiving tubes. Light from the strobe passes through the tube, where it changes intensity as it is both refracted by the interfaces and absorbed by the fluid media. A linear array of 1024 diodes (pixels) in the line camera records the varying light intensities along the length of the collection tube. A sketch of the centrifuge bucket system appears in Figure 1.

These intensities are passed to the data acquisition system as digitized values, as shown in Figure 2. This plot shows light intensity at each position along the array. The first drop in light intensity is due to a sharp calibration mark etched on the collection tube. The medium inside the tube, on either sides of the first calibration mark, is water, which provides a relatively constant light level until the water/oil interface is reached. A dye has been placed in the collection bucket to color the oil and causes a sharply reduced light level. No dye is necessary when using reservoir crude oils. The light level increases to the right at the oil/air interface. The second calibration mark causes the intensity drop, just before the end of the bucket slot.

From a data array such as this, the oil and water production can be determined at the moment the picture was taken. Pictures such as this are taken of all six buckets on the rotor in a single second. At each speed, approximately 800 to 1000 pictures are taken of each bucket. Most of the noise seen in the digital data (Figure 2) is due to surface imperfections of the collection tube.

A pixel corresponds to 4 μl, which is a factor of 10 more precise than the volumes that could be read by the eye. At this level of precision, and with the ability to rapidly sample the collection tubes, high quality transient volumetrics were recorded at each rotation speed. Corrections for rotor wobble induced magnification error and collection bucket deformation volumetric error are obtained from calibration runs and incorporated into the data analysis software.

For gravity drainage studies on the ultracentrifuge, one-inch long, one-inch diameter core plugs were used. Bulk volumes, porosities and air permeabilities were measured before shrink wrapping with rubber and teflon sleeves. The core samples were then mounted in Hassler cells, evacuated and saturated with degassed synthetic brine. Brine permeabilities were also measured prior to removing the cores from Hassler cells. Brine saturated core samples were placed in centrifuge drainage buckets, and surrounded with oil. Degassed Soltrol 170 was used as the oil phase. The buckets were loaded into the ultracentrifuge and spun at a speed of just under 12,000 rpm for at least 72 hours. This was the 'oil flush' in which oil replaced brine until an irreducible water saturation was attained. The volume of water produced during this primary drainage process defined the OOIP for the gravity drainage experiment. The amount of water saturation at the end of a primary drainage experiment can be controlled by suitably selecting the rotation speed and the spinning time. The samples were then removed from the drainage buckets and mounted in Hassler cells to measure permeability to oil phase in the presence of irreducible water saturation. The core samples were reloaded into a fresh set of drainage buckets. A small quantity of brine was added to each collection tube to move the oil-water interface slightly above the bottom of the scale. The core samples, surrounded by air, are now ready for gravity drainage. The centrifuge was rotated at different speeds in ascending order. The speeds were selected to cover the entire rotation range of the ultracentrifuge, and were equal on a logarithmic scale. The samples were spun at each speed for at least 24 hours. Low permeability samples were spun for even longer times. Both the amount of oil and the amount of brine produced at different times were recorded.

THEORY

The fluid flow equations pertaining to gravity drainage in an ultracentrifuge differ from the standard multi-phase flow equations in two ways. First, the 'gravitational' acceleration is position dependent. Second, the invading fluid (gas) can be treated as having negligible viscosity (infinite mobility), relative to the oil phase. For the case of two incompressible mobile phases (oil, gas) the equations may be written in IMPES form as an equation for conservation of mass for oil,

$$\phi \frac{\partial S_o}{\partial t} + \frac{\partial V_o}{\partial x} = 0, \qquad (18)$$

and an equation for oil flux, V_o,

$$v_o = \frac{\lambda_o}{\lambda} v \quad - \quad \frac{\lambda_o \lambda_g}{\lambda} \cdot \frac{\partial \Phi_c}{\partial r} \cdot \tag{19}$$

In the above equation, λ_o and λ_g are the mobilities of oil and gas phase respectively and λ is the total mobility. The convective (first) term is proportional to a total flux, V, given by

$$v \cdot \int_{r_1}^{r_2} \lambda^{-1} \, dr \quad = \quad - \int_{r_1}^{r_2} \frac{\lambda_o}{\lambda} \cdot \frac{\partial \Phi_c}{\partial r} \, dr \, . \tag{20}$$

A pseudo-pressure, Φ_c, defined as

$$\Phi_c = \frac{1}{2} \Delta\rho \, (r_a^2 - r^2) \, \omega^2 - P_c(S_o) \tag{21}$$

has been introduced. It is the sum of the buoyancy and the capillary forces. The former drives the fluid motion and the latter impedes it. At equilibrium, $\Phi_c = 0$ throughout the core. The boundary conditions are those of a gas flood at the inlet and vanishing capillary pressure at the outlet.

$$v_o = 0, \text{ at } r = r_b \text{ (inlet)} \tag{22a}$$

$$\Phi_c = 0, \text{ at } r = r_a \text{ (outlet)} \tag{22b}$$

The initial condition (t=0, ω=0) assumes capillary equilibrium throughout the core, $P_c(S_o) = 0$. In the limit of negligible gas viscosity, $\lambda_g >> \lambda_o$, the expression for oil flux simplifies to

$$v_o = - \lambda_o \cdot \frac{\partial \Phi_c}{\partial r} \cdot \tag{23}$$

The convective term is negligible because V remains finite in this limit. Physically, this limit states that the oil mobility is the rate limiting step in the gravity drainage process. The gas phase simply moves into the volume vacated by the oil.

Equations (18) through (23) are in the form of a nonlinear diffusion equation for $S_o(r,t)$. The equations are spatially discretized on an equally spaced point distributed grid, with first and last grid points at the boundaries. The inlet boundary condition is treated by reflection, and the outlet by fixing the saturation (such that P_c vanishes). Mobilities are evaluated at the block faces, with saturations interpolated from the adjacent nodes. This central difference form may be used since the equations are parabolic and not hyperbolic. The equations are discretized in time using Crank-Nicholson's semi-implicit formulation. The resulting set of algebraic equations are solved iteratively using a finite difference Levenburg-Marquardt algorithm. This method for solution of nonlinear systems shifts from a steepest-descent method far from the solution to a Newton's method in the vicinity of the solution.

AUTOMATIC HISTORY MATCHING SIMULATOR

An automatic history matching simulator was developed to obtain oil relative permeability information from transient production data collected during a multi-stage gravity drainage ultracentrifuge experiment. The automatic history matching simulator has two parts. One is the centrifuge gravity drainage simulator described in the previous section and the other part is a nonlinear optimization program (outlined in the Appendix) which uses the method of rotational discrimination [25,26] for parameter estimation. Given a capillary pressure curve, the automatic history matching algorithm searches for an oil relative permeability curve that results in a best fit, in a least squares sense, between the observed behavior of the experiment and the calculated behavior of the ultracentrifuge gravity drainage simulator. The automatic history matching algorithm has been tested on synthetic data generated using the simulator for which the solution is known. The history matching simulator also has the capability of determining both capillary pressures and relative permeabilities simultaneously from the production history of the experiment.

DATA ANALYSIS PROCEDURE

Capillary pressure curves can be determined directly from a Hassler-Brunner type analysis if each stage of the experiment is carried out to equilibrium. However, production from low permeability rock samples and core samples with significant microporosity, may suffer from very long equilibration times. Figure 6 shows the final 10 days of production data for Berea sandstone and reservoir rock samples during an intermediate stage of a gravity drainage process in the centrifuge. Oil production data, when plotted as a function of logarithmic time clearly indicates a lack of equilibrium even after twenty four hours of production. In most cases, it may not be practical to conduct the experiment until equilibrium is reached. Also when the produced volume is small, the volumetric measurement system may not have the resolution to accurately record the production data.

Optimal extrapolation has been obtained from a stretched exponential function:

$$v_p = a - b \cdot e^{-(t/\tau)^{\beta}} \qquad (24)$$

where v_p is the total volume produced by time t. Parameters a, b, τ and β are to be estimated by fitting the exponential function to the tail-end portion of the production curve. The parameter a is the best fit estimate for the equilibrium production; τ is a measure of the decay time.

An asymptotic (long time, Laplace transform) analysis of the potential Φ_c linearized about $\Phi_c = 0$, shows that v_p decays as a superposition of exponentials. The superposition may be represented by a single stretched exponential, since the decay rates occur over a broad spectrum. The local decay rate in the core is given by $\lambda_o \cdot dPc/dS$, which varies as a function of saturation throughout the core.

The exponent β must be calibrated by a long time experiment. In our experience, a value of $\beta = 0.77$ has represented both bi-modal reservoir rock and Berea sandstone. The ten day data sets, and exponential fits are shown in Fig.6. The fits are obtained from the first day of data, only. The use of a simple exponential provides a good extrapolation of the data only for three days. This is true of both the Berea (Fig.6a) and the reservoir core sample (Fig.6b). However, for both samples, the stretched exponential at $\beta = 0.77$ provides an extrapolation from one day data to ten day data.

Time transient plots of average oil saturation are shown in Fig.7, again for reservoir core samples. This is a cross-plot of 4 hour and 24 hour saturations against the extrapolated value. Both times have been suggested as adequate for equilibrium to occur [19]. Equilibrium is indicated by a straight line of slope one. The same data is plotted as a function of rotation rate in Fig.8. It is seen that equilibrium is not attained at the highest rates (lowest saturations), and that unlike Berea, there is still significant saturation change underway. It should be noted that without the volumetric precision provided by the automated system, that both systems would have been judged to have reached equilibrium after 24 hours.

Parameter estimation requires a representation of the capillary pressure function. As a first step, capillary pressure points are determined from the multi-stage centrifuge production data (extrapolated to equilibrium) using the generalized Hassler-Brunner analysis described earlier. The improved Hassler-Brunner analysis includes the variation in centripetal acceleration through the length of the core sample and desaturation effects at high rotation rates. For these drainage experiments, there is no evidence for capillary desaturation. This is evident in Fig.8 where the data remains concave up on a semi-logarithmic plot.

One capillary pressure point, referred to hereafter as a Hassler-Brunner point, is obtained for every stage of the experiment in this manner. An estimate of the entire capillary pressure curve may be obtained by requiring mass balance consistency at each stage of the experiment. The function S(Pc) is constructed from piecewise quadratic polynomial functions. If the resulting capillary pressure curve is not monotonically decreasing with increasing wetting phase saturation, i.e. if $dS(P_c)/dP_c > 0$, then the Hassler-Brunner points are adjusted until $dS(P_c)/dP_c = 0$. Cubic and higher order polynomial functions have been examined, and do not perform as well. They usually resulted in non-monotonic and physically unacceptable shapes for capillary pressure, as there is not sufficient information in the experiment to uniquely determine the curves.

To use the parameter estimation (or nonlinear regression) technique for determining relative permeabilities, one must choose functional representations of the relative permeability curves. Kerig and Watson [27] and Watson et.al. [28] have addressed the functional representation aspect of the parameter estimation problem in detail. They have shown that a simple Corey exponent type relative permeability can result in large bias errors in the estimation. Bias error is the result of an inadequacy in the flexibility of the assumed functional form to represent the true relative permeability curve. To obtain more accurate estimates of relative permeabilities, it is necessary to use more flexible functional forms, and in general utilize more parameters. In general, as the number of parameters increases, the variance error, or the statistical uncertainty in the estimates, will also increase. On the

other hand, fewer parameters may result in large bias error. The optimal functional forms will be those that minimize the combination of these two errors.

In this work the relative permeability curves are parameterized in tabular form by specifying values at selected saturations. These points are referred to as "knots". The user can specify the number of knots on each curve and their locations. Some of the knots may be fixed based on prior experimental information (e.g., end point relative permeabilities) and the rest will be free parameters to be determined by history match. Once the knots are specified, a complete curve can be generated through smooth interpolation.

After the best fit relative permeability curve has been determined, the program calculates confidence limits on the estimated parameters using statistical methods outlined in the Appendix. These confidence limits are useful in making appropriate parameter selections and in judging the quality of the results.

RESULTS AND DISCUSSION

In this section we demonstrate our parameter estimation procedure with laboratory gravity drainage data obtained using one-inch diameter, one-inch long, approximately 200 mD (permeability to brine) Berea core samples. An initial water saturation of 14% was established by performing a centrifuge oilflush at 11800 rpm for twenty four hours. Gravity drainage was performed by increasing the rotation rate in ten distinct steps, starting from 500 rpm. The highest speed was 11800 rpm and the intermediate speeds were equally spaced on a logarithmic scale. The core samples were held at each speed for approximately twenty four hours. The position of the water/oil and the oil/air interfaces were continuously monitored and stored as a function of time from which cumulative volumes of oil and water produced are calculated. Shown in Fig.9 is a typical plot of cumulative oil production from a Berea core sample, at ten different rotation rates.

In this case, data from the first six stages of the experiment were used for parameter estimation. Data beyond the sixth stage showed very little oil production, with the average oil saturation dropping below one tenth of a percent. Average equilibrium saturations are calculated for each stage of the experiment by stretched exponential extrapolation at $\beta = 0.77$. Discrete Hassler-Brunner points were determined; material balance requirements and monotonicity constraints were used to construct a capillary pressure function.

Optimization Procedure I utilizes the capillary pressure curve as a fixed input in the history matching process for oil relative permeabilities. Four parameter points (knots) were selected to represent the oil relative permeability curve. Using four parameter points we were able to generate monotonic relative permeability curves for which a reasonable match of the data was obtained, as shown in Fig.9. The best-fit relative permeability curve with four parameter points is shown in Figs. 11 and 12. Also shown are the approximate 95% confidence intervals for the history-matched parameters. In Fig.12 the intervals are smaller than the graphics symbols. Fig.11 shows a linear extrapolation of the oil relative permeability to 100% saturation, providing a consistency check of the

method. Although the oil permeability was measured at the initial oil saturation, it was not necessary to utilize this information to obtain a well determined relative permeability.

Increasing the number of parameter points for this case (six points, Fig.13) resulted in no significant improvement in the quality of history match, but increased the statistical uncertainty in the parameter estimates. This indicates that for this data set, the relative permeability curve may already be well represented with four parameter points. Examination of the magnitude of the error bars can be used to determine whether additional parameter points are required, and if so their most useful locations. They may also be used to show if any of the existing parameter points are redundant, as is the case in Fig.13. Fig.13 also utilized different locations for the parameter points; the two curves are within the estimated error bars for the parameters.

Let's discuss the quality of history match stage by stage. The first stage of the experiment indicates a delay in production compared to the simulation results. At the beginning of the experiment, the gas saturations are very low and the assumption of infinite mobility for the gas phase may not be valid. At low gas saturations, the gas phase pressure gradients are finite and will exert a viscous drag in the oil phase. As pointed out by Nordvedt et.al. [15] in the region of low gas saturation there is sufficient sensitivity to determine gas relative permeability accurately. Also, in this region the assumption of infinite gas mobility may result in incorrect estimates for oil relative permeability. As the gas saturation increases, the gas phase mobility rapidly increases to be at least two orders of magnitude larger than the oil phase mobility. The gas mobility will not affect the calculation of oil relative permeabilities. In the region of low gas saturation, a good strategy would be to fix oil relative permeability through independent measurements and history match for gas permeability only.

The quality of history match is excellent for the second and third stages of the experiment, not as good for the fourth, and is again quite good beyond that. This seems to be consistent throughout all the data sets we have analyzed, for both Berea and reservoir samples. The simulations indicate rapid attainment of mechanical equilibrium compared to the experimental data. Lack of fit is believed to result from the representation of Pc beyond stage 3 (1000 rpm) of the experiment. The asymptotic solution for the flow potential, Φ_c, indicates that the decay of Φ_c to $\Phi_c = 0$ is controlled by the product $\lambda_o \cdot dP_c/dS$. Errors in capillary pressure gradient cannot be easily compensated for by a monotonic λ_o during the history match.

Beyond the third stage the system enters the "elbow" portion of the P_c curve, where dP_c/dS starts increasing rapidly with saturation. Incorrect representation of the shape of the P_c curve will result in incorrect estimates of equilibration times. Determining the capillary pressure curve through material balance is not unique; imposing the condition that the calculated P_c curve should satisfy mass is necessary, but not a sufficient condition. Beyond the fourth stage, the equilibration time is still underestimated, but it is no longer critical to the goodness of fit. Here the capillary pressure curve is increasing very steeply, while the saturation range is quite limited.

An attempt to better determine the P_c curve in the "elbow" region was addressed by simultaneously history matching the production data with both relative permeability and capillary pressure as parameters (Procedure II). The capillary pressure curve is parameterized in tabular form by specifying values at five selected saturation parameter points. Intermediate points were obtained using cubic spline interpolants in logarithmic coordinates. The Hassler-Brunner points provided a starting guess for P_c. History match was performed, and the results are shown in Fig.14. The estimated capillary pressure and relative permeability curves are shown in Figs. 15 and 16, respectively.

It is apparent that the overall pattern of the history match is quite similar with the two procedures (Figs. 9 and 14). However, the fixed Pc approach (Procedure I) actually provided a more accurate match. Of course, with half as many parameters for optimization, the calculation was much quicker as well. The capillary pressure curve (Fig.15) shows the inability of smooth functional forms, even tabular ones, to represent the sharp elbow of the Pc curve. The resulting function does not provide a physically reasonable estimate of capillary pressure. However, in the upper saturation ranges, both Pc curves are smooth, and are in excellent agreement. Beyond the elbow, the Hassler-Brunner points will describe the steep capillary pressure curve. No information is available from the history matching procedure.

The implications of the two representations of the Pc curve on relative permeability are shown in Fig.16. For saturations above 30%, both Pc curves agree, and so do the relative permeability estimates. However, at lower saturations, the curves may disagree by as much as an order of magnitude. Based on goodness of fit values, and a recognition of the poor Pc representation in Procedure II, our belief is that the curves generated by Procedure I are more accurate. In applications with reservoir samples, the capillary pressure curve increases more gradually. In this case the two methods are in excellent agreement.

SUMMARY

A review of methods for obtaining capillary pressure from equilibrium centrifuge data has been presented, emphasizing the direct construction (non-parametric) methods. An exact solution is obtained and presented in a standard form. The approximate methods that have appeared in the literature, ranging from Hassler-Brunner (1948) [1] to Rajan (1986) [6], have been re-formulated in this standard form, for comparison.

The use of an automated centrifuge has been presented, and its value indicated for providing high quality time production data over extensive time intervals. Standard experimental procedure involves monitoring six cores, possibly each second, with 4μl precision, for a ten stage experiment, each stage lasting for one day.

A three week decay study has been performed, with ten days of data acquired at the highest rotation rate. It has been shown that a stretched exponential, with stretch parameter $\beta = 0.77$ is effective in extrapolating one day experimental results to at least the ten day interval, for both

reservoir core samples, and Berea sandstone. Extrapolation from the first four hours of data was unable to predict the ten day response.

It is recommended that standard procedure utilize 24 hour data, as shorter intervals appear inadequate, and that data be extrapolated utilizing a stretched exponential. If it is not possible to calibrate samples independently, the value of $\beta = 0.77$ may be used.

Two parameter estimation procedures for determining relative permeability have been presented. In the first, capillary pressure is fixed, and determined by the above methods. In the second, capillary pressure is allowed to vary during the parameter estimation. It has been shown that the parameter estimation technique provides a poor estimate of Pc(S), when that curve has a sharp "elbow", even though a good fit is obtained for the production curve. The inability to adequately represent Pc(S) is not as critical for samples with a wider pore size distribution, and a broad elbow, as typified by our reservoir rock samples.

Inadequacies in Pc(S) introduce biases into the relative permeability. Once saturations are sufficiently low to enter the "elbow" of the capillary pressure curve, up to an order of magnitude difference has been found between the two optimization procedures.

It is recommended that Pc(S) be fixed, not variable, as an optimization procedure will be able to bias the relative permeability to compensate for errors in Pc. In addition, this procedure is computationally more efficient.

The use of a statistical method to estimate errors and sensitivities is critical for guiding a parameter estimation approach. The method of rotational discrimination [24-26] performs such an analysis, and uses this information during the optimization to identify the dominant combinations of parameters.

ACKNOWLEDGEMENTS

The authors thank J. W. Jennings, Jr. for providing the nonlinear optimization code, I. Mrosovsky for his technical direction, and BP America for permission to publish this paper. One of us (MJK) thanks K. G. Ayappa and A. D. Gupta for stimulating technical discussions.

NOMENCLATURE

a	parameter in Eqn. (24)
b	parameter in Eqn. (24)
N_B	Bond number, dimensionless
P_c	capillary pressure, psi
r	distance from the axis of rotation to a point within the core, cm
r_a	distance from the axis of rotation to furthest point of the core, cm
r_b	distance from the axis of rotation to closest point of the core, cm

$\langle S \rangle$	experimentally observed average saturation
$\langle S \rangle_0$	experimental average saturation with zero length correction
S_b	saturation at the inlet end of the core sample
S_{HB}	Hassler-Brunner saturation
S_o	saturation of oil phase
t	time, sec
V_o	superficial velocity of oil phase, cm/sec
V	total superficial velocity, cm/sec
v_p	cumulative volume produced in centrifuge by time t, cc
$W(z)$	length correction factor in exact solution
$\rho(z)$	length correction factor in Rajan's approximate solution
z	fractional capillary pressure, dimensionless
β	parameter in Eqn.24
ϵ	centrifuge geometry factor, dimensionless
λ_o	mobility of oil phase
λ	total mobility
Φ_c	pseudo-pressure, psi
$\Delta\rho$	fluid density difference, positive, gm/cc
τ	decay time constant in Eqn. (24), sec
ω	rotation rate, rpm

REFERENCES

1. Hassler, G.L., and Brunner, E. : "Measurement of Capillary Pressures in Small Core Samples," Trans. AIME (1945) **160**,114-123.

2. Hoffman, R.N. : "A Technique for the Determination of Capillary Pressure Curves Using a Constantly Accelerated Centrifuge," SPEJ (Sept. 1963) 227-235.

3. Luffel, D.L. : "Further Discussion of Paper Published in SPEJ, Sept. 1963 (A Technique for the Determination of Capillary Pressure Curves Using a Constantly Accelerated Centrifuge, by R.N. Hoffman)," SPEJ (1964) **4**,191-194.

4. van Domselaar, H.R. : "An Exact Equation to Calculate Actual Saturations From Centrifuge Capillary Pressure Measurements," Rev. Tec. Intevep (1984) **4**, 55-62.

5. Melrose, J.C. : "Interpretation of Centrifuge Capillary Pressure Data," paper presented at the SPWLA 1986 Annual Logging Symposium, June 9-13.

6. Rajan, R.R. : "Theoretically Correct Analytical Solution for Calculating Capillary Pressure - Saturation From Centrifuge Experiments," paper presented at the SPWLA 1986 Annual Logging Symposium, June 9-13.

7. King, M.J., et al. : "Simultaneous Determination of Residual Saturation and Capillary Pressure Curves Utilizing the Ultracentrifuge," paper SPE 15595 presented at the 1986 SPE Annual and Technical Conference and Exhibition, New Orleans, LA, Oct. 5-8.

8. Ayappa, K.G., et al. : "Capillary Pressure: Centrifuge Method Revisited," AIChE Journal (March 1989) **35**, 365.

9. Christiansen, R.L., and Cerise, K.S. : "Capillary Pressure: Reduction of Centrifuge Data," paper presented at the AIChE 1987 National Meeting, New York City, Nov. 15-20.

10. Bentsen, R.G., and Anli, J. : "Using Parameter Estimation Techniques to Convert Centrifuge Data Into a Capillary-Pressure Curve," SPEJ (February 1977), 57-64.

11. Wunderlich, R.W. : "Imaging of Wetting and Nonwetting Phase Distributions: Applications to Centrifuge Capillary Pressure Measurements," paper SPE 14422 presented at the 1985 SPE Annual Technical Conference and EXhibition, Las Vegas, Sept. 22-25.

12. Morrow, N.R., and Songkran, B : "Effect of Viscous and Buoyancy Forces of Nonwetting Phase Trapping in Porous Media," in Surface Phenomena in Enhanced Oil Recovery, ed. by D.O. Shah, Plenum Press, New York, 1981, 384-411.

13. O'Meara, D.J., and Crump, J.G. : "Measuring Capillary Pressure and Relative Permeability in a Single Centrifuge Experiment," paper SPE 14419 presented at the 1985 SPE Annual and Technical Conference and Exhibition, Las Vegas, NV, Sept. 22-25.

14. Firoozabadi, A., and Aziz, K. : "Relative Permeability from Centrifuge Data," paper SPE 15059 presented at the 1986 California Regional Meeting, Oakland, CA., April 2-4.

15. Nordvedt, J.E., Watson, A.T., Mejia, G., and Yang, P. : "Estimation of Capillary Pressure and Relative Permeability Functions from Centrifuge Experiments," unsolicited paper SPE 20805, (1989).

16. Bruce, W.A., and Welge, H.J. : "The Restored State Method for Determination of Oil in Place and Connate Water," Drilling and Prod. Prac. API (1947), 166-174

17. Melrose, J.C. : "Use of Water Vapor Desorption Data in the Determination of Capillary Pressures at Low Water Saturations," SPERE (Aug. 1988), 913-918

18. Purcell, W.R. : "Capillary Pressures - Their Measurement Using Mercury and the Calculation of Permeability Therefrom," Trans. AIME (1949) **186**, 39-48.

19. Omoregie, Z.S. : "Factors Affecting the Equivalency of Different Capillary Pressure Measurement Techniques," SPEFE (March 1988), 147-155.

20. Johnson, E.F., Bossler, D.P., and Naumann, V.O. : "Calculation of Relative Permeability from Displacement Experiments," Trans. AIME (1959) **216**, 370-378.

21. Batycky, J.P., McCaffery, F.G., Hodgins, P.K., and Fisher, D.B. : "Interpreting Capillary Pressure and Rock Wetting Characteristics From Unsteady State Displacement Measurements," paper SPE 9403 presented at the 1980 SPE Annual and Technical Conference and Exhibition, Dallas, TX, Sept. 21-24.

22. King, M.J., and Dunayevsky, V.A. : "Capillary Corrections to Buckley - Leverett Flow," submitted to Transport in Porous Media.

23. Hagoort, J. : "Oil Recovery by Gravity Drainage," SPEJ (June 1980), 139-150.

24. Jennings, J.W. Jr., Mcgregor, D.S., and Morse, R.A. : "Simultaneous Determination of Capillary Pressure and Relative Permeability by Automatic History Matching," paper SPE 14418 presented at the 1985 SPE Annual and Technical Conference and Exhibition, Las Vegas, NV, Sept. 22-25.

25. Jennings, J.W. Jr. : "A Method for Measuring Capillary Pressures and Relative Permeabilities Based Upon a Transient Analysis of a Rapid Restored-State Experiment,: Ph.D. Dissertation (1984), Texas A&M University, College Station, Texas.

26. Law, V.J., and Fariss, R.H. : "Transformational Discrimination for Unconstrained Optimization," Ind. Eng. Chem. Fundam. (1972) **11**, 154-161.

27. Kerig, P.D. and Watson, A.T. : "Relative Permeability Estimation From Displacement Experiments - An Error Analysis," SPERE (March 1986) 175-182.

28. Watson, A.T. et.al. : "A Regression-Based Method for Estimating Relative Permeabilities From Displacement Experiments," SPERE (Aug. 1988) 953-958.

29. Himmelblau, D.M. : "Process Analysis by Statistical Methods," Sterling Swift, Austin, Texas (1970) 197.

APPENDIX - AUTOMATIC HISTORY MATCHING ALGORITHM

Cumulative produced volume from the centrifuge is measured at a set of discrete times giving:

$$\bar{V}^{obs} = \left[V_1^{obs}, V_2^{obs}, V_3^{obs} \ldots . V_m^{obs} \right] \qquad \text{(A1-1)}$$

where V_i^{obs} is the observed cumulative production at time t_i and m is the number of observations. The simulator calculates the cumulative production at the same set of times for a given set of capillary pressure and relative permeability data resulting in

$$\bar{V}^{cal} = \left[V_1^{cal}(\bar{X}), V_2^{cal}(\bar{X}), \ldots . V_m^{cal}(\bar{X}) \right], \qquad \text{(A1-2)}$$

where X is a vector composed of n parameters describing the capillary pressure and relative permeability curves.

The objective of the history matching algorithm is to find X such that the objective function,

$$Q(\bar{X}) = \sum_{k=1}^{m} R_k^2(\bar{X}), \qquad \text{(A1-3)}$$

is minimized. The residuals R_k are defined by

$$R_k(\bar{X}) = W_k \left(V_k^{obs} - V_k^{cal}(\bar{X})\right), \qquad \text{(A1-5)}$$

where W_k is a user-supplied weighting factor. The solution of the minimization problem, $X = X^*$, is found using the method of rotational discrimination. The method of rotational discrimination is best thought of as a modification of the Gauss-Newton method. It uses Newton's method in a rotated space generated by the eigenvectors of the Hessian or second derivative matrix of **Q**. The eigenvectors of the Hessian matrix are the principal axes of the paraboloid that approximates **Q**. The eigenvalues of the Hessian are the second derivatives of the paraboloid in the eigenvector direction. The search vector is computed in the rotated (eigenvector) coordinate system.

There are a number of reasons for using this new coordinate system. Law and Fariss[26] refer to this rotated coordinate system as "non-interacting". In other words, the change in **Q** caused by moving a certain distance in one of the eigenvector directions is independent of the distances moved in the other eigenvector directions. This is particularly useful when null-effect parameters are present. Null-effect vectors can be easily detected by comparing the magnitude of the eigenvalues. Any eigenvalue which is many orders of magnitude smaller than the largest eigenvalue indicates that **Q** is nearly flat and any move in the corresponding eigenvector direction will be null-effect. It is usually a good strategy to not move at all in this direction. The Gauss-Newton method will usually produce very large moves in the null-effect directions. Also, Newton's method is not amenable to the consideration of each parameter separately. All parameters must be considered simultaneously.

In addition to estimating the parameters in a nonlinear model an approximate confidence region, ellipsoidal in shape, can be estimated for all the parameters using the following equation[25,29]:

$$(\bar{X}^C - \bar{X}^*) \cdot G \cdot (\bar{X}^C - \bar{X}^*)^T = \sigma^2 n F_{1-\alpha}(n,m-n) \qquad \text{(A1-6)}$$

where $F_{1-\alpha}(n,m-n)$ is the upper limit of the F-distribution for a confidence level of α and (n,m-n) degrees of freedom, and σ^2 is the sample variance of the residuals at the minimum of **Q**. The matrix **G** is a symmetric nxn matrix defined by

$$G_{ij} = \sum_{k=1}^{m} \frac{\partial R_k}{\partial X_i} \frac{\partial R_k}{\partial X_j} \qquad \text{(A1-7)}$$

In Eqn. (A1-6) X^C is the approximate joint confidence region for the the estimated parameters X^*.

King et.al. (1986)

$$S_b(\omega^2) = \frac{2r_b}{r_a + r_b} \cdot S_{HB}(\omega^2) + \left[\frac{r_a^2 - r_b^2}{2 r_b^2}\right] \int_0^1 dz\ W(z)\ S_{HB}(z\omega^2)$$

Hassler, Brunner (1948)

$$S_b(\omega^2) \simeq 1 \cdot S_{HB}(\omega^2) + 0$$

Hoffman (1963)

$$S_b(\omega^2) \simeq \frac{2r_b}{r_a + r_b} \cdot S_{HB}(\omega^2) + 0$$

van Domselaar (1984)

$$S_b(\omega^2) \simeq \frac{2r_b}{r_a + r_b} \cdot S_{HB}(\omega^2) + \left[\frac{r_a^2 - r_b^2}{2 r_b^2}\right] \int_0^1 dz\ \bar{W}\ S_{HB}(z\omega^2)$$

Rajan (1986)

$$S_b(\omega^2) \simeq \frac{2r_b}{r_a + r_b} \cdot S_{HB}(\omega^2) + \left[\frac{r_a^2 - r_b^2}{2 r_b^2}\right] \int_0^1 dz\ \rho(z)\ S_{HB}(z\omega^2)$$

$$\rho(z) = \frac{2 r_b^2}{r_a(r_b - r_a)} \ln\left[\frac{2\sqrt{1+\epsilon z}}{1+\sqrt{1+\epsilon z}}\right] - \frac{(r_b - r_a)(1+\epsilon)}{r_a \cdot (1+\epsilon z)} \left\{\frac{z\left(1+\sqrt{1+\epsilon}\right)}{\left(1+\sqrt{1+\epsilon z}\right)}\right\}^2$$

Table 1 - Summary of Capillary Pressure Analyses in Standard Form
Symbols and Functions Defined in Text

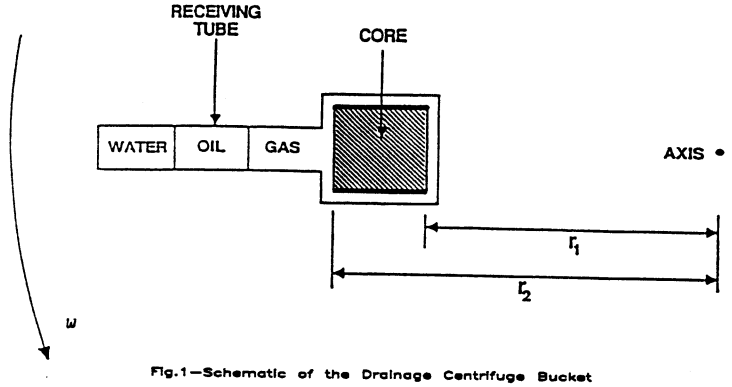

Fig.1—Schematic of the Drainage Centrifuge Bucket

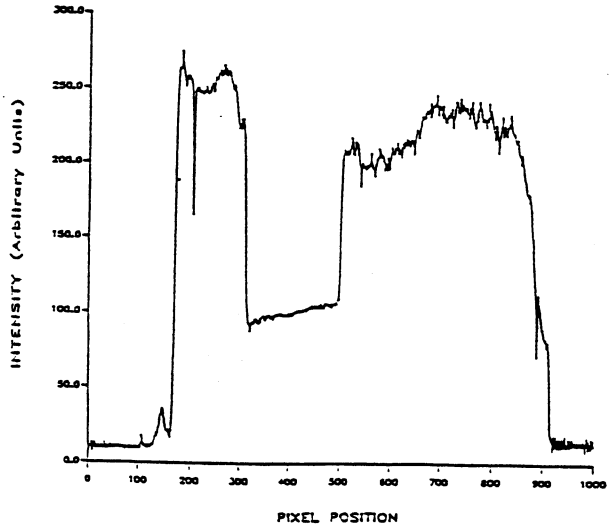

Fig.2—Collection Tube Intensity Trace

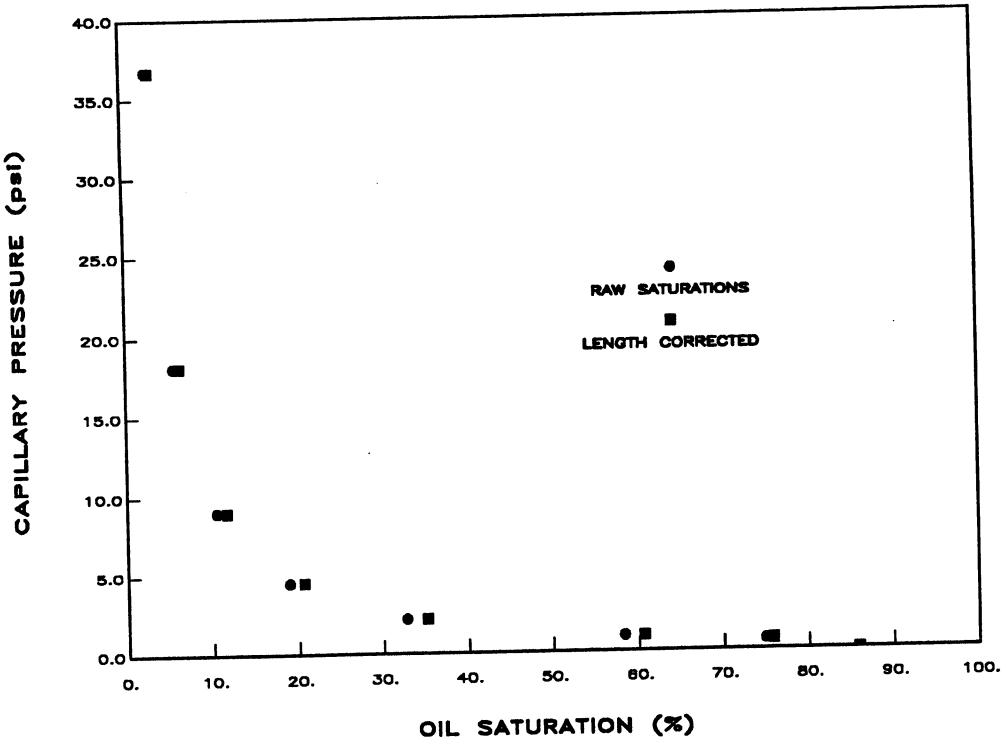

Fig.3—Experimental Saturations Corrected for Finite Core Length

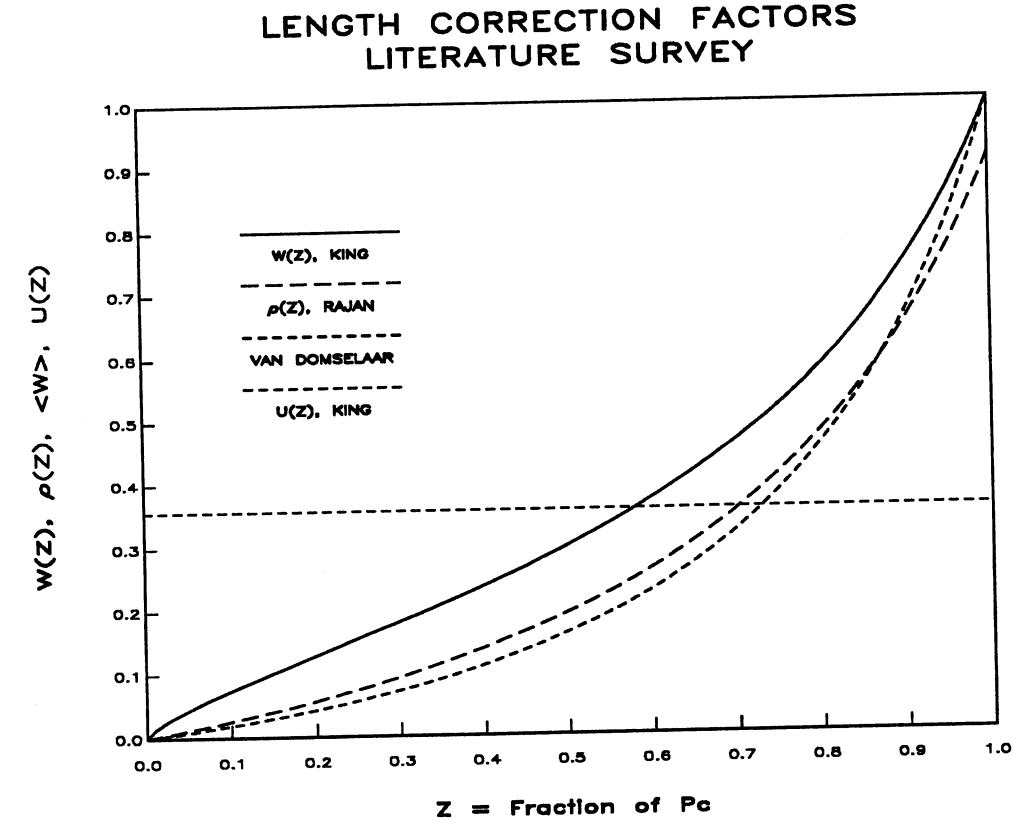

Fig.4—Comparison of King, Rajan, van Domselaar

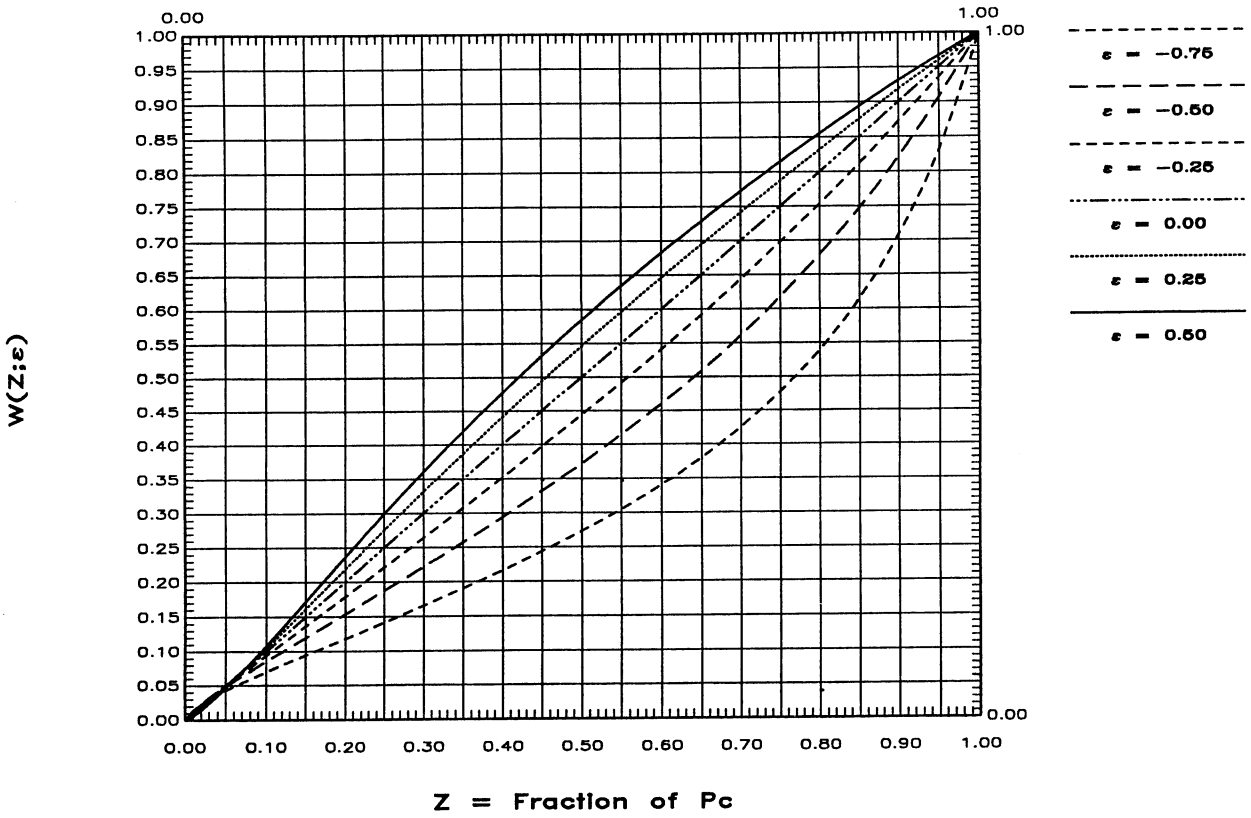

Fig.5—Finite Length Correction Type Curves

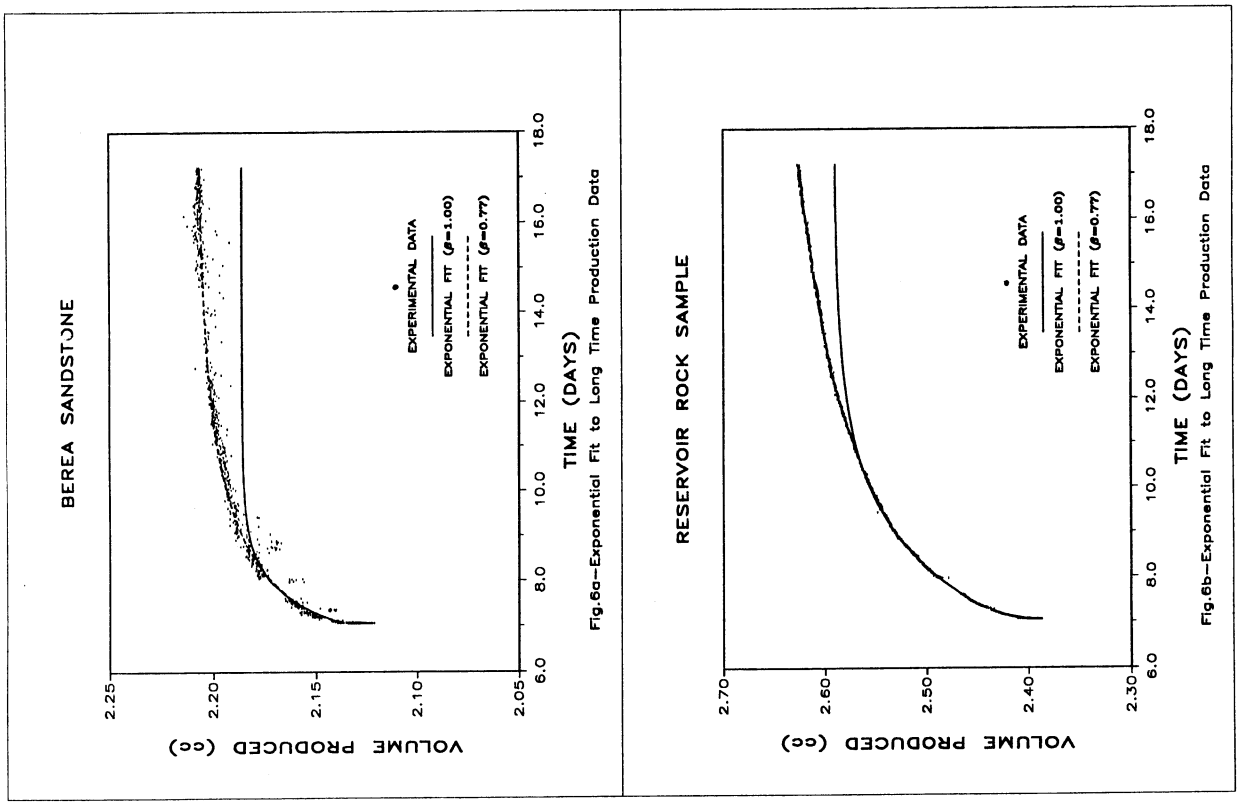

Fig.6a—Exponential Fit to Long Time Production Data

Fig.6b—Exponential Fit to Long Time Production Data

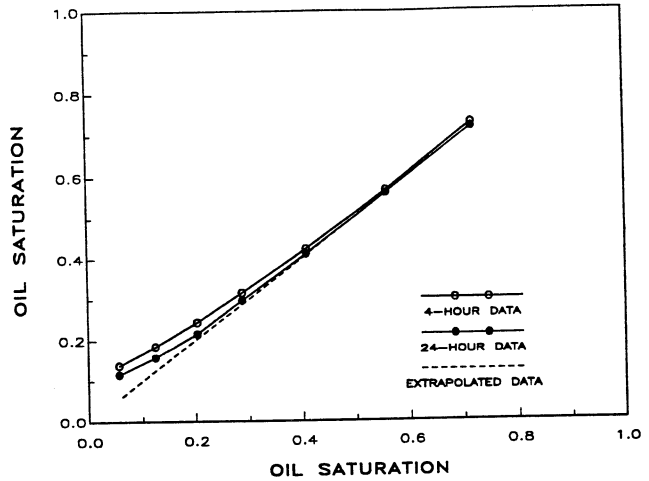

Fig.7—Experimental End Point Saturation Data Compared to Extrapolated Data

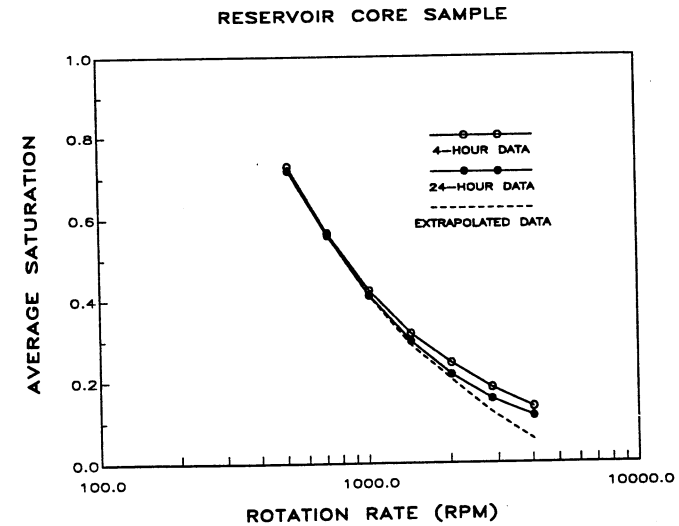

Fig.8—Average Saturation as a Function of Rotation Rate

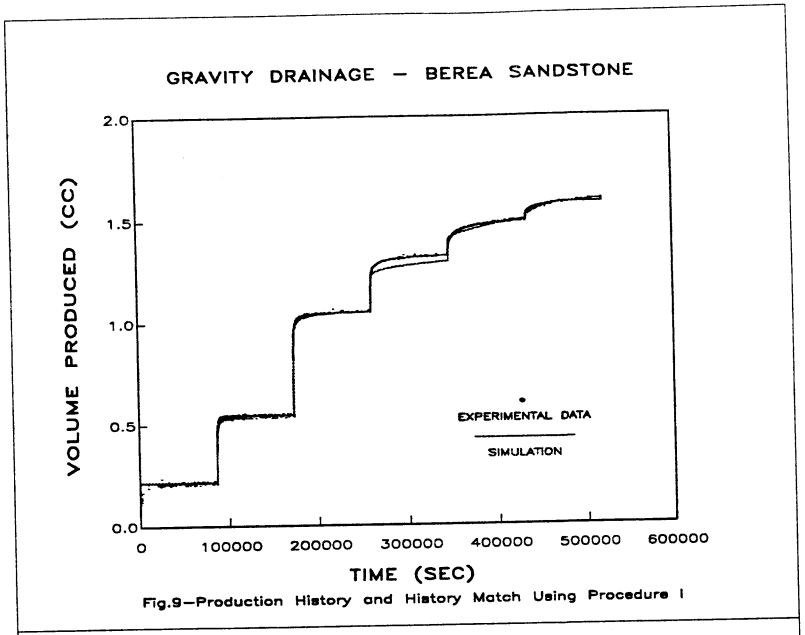

Fig.9—Production History and History Match Using Procedure I

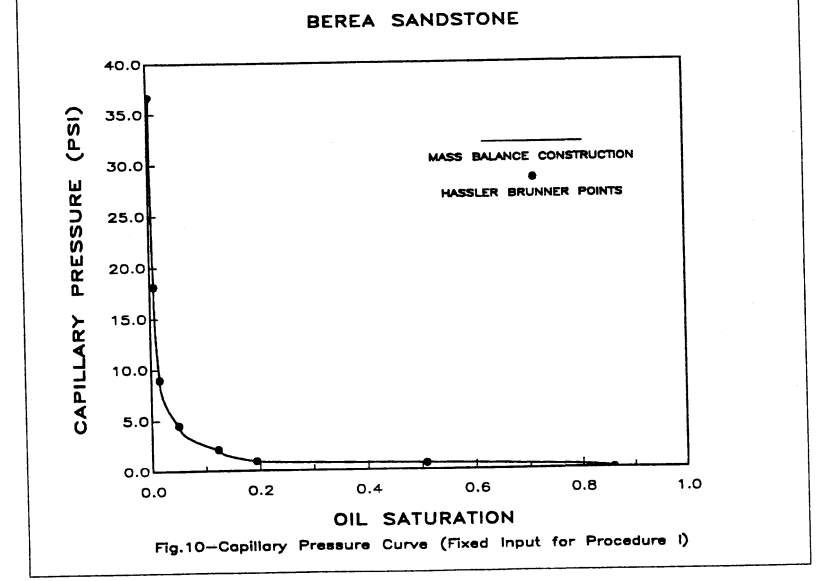

Fig.10—Capillary Pressure Curve (Fixed Input for Procedure I)

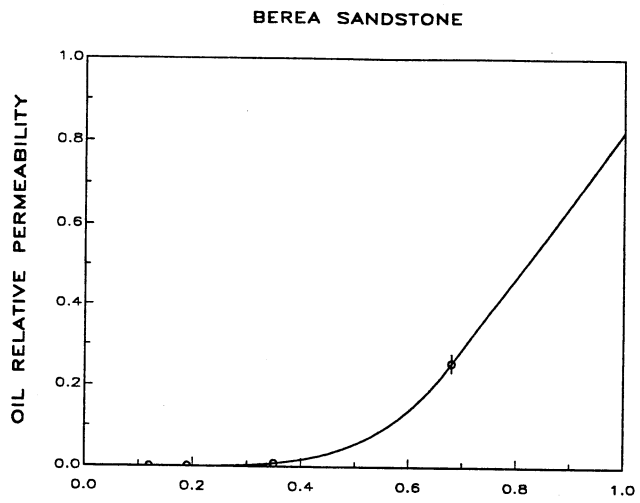

Fig.11—Estimated Oil Relative Permeability Curve Using Procedure I

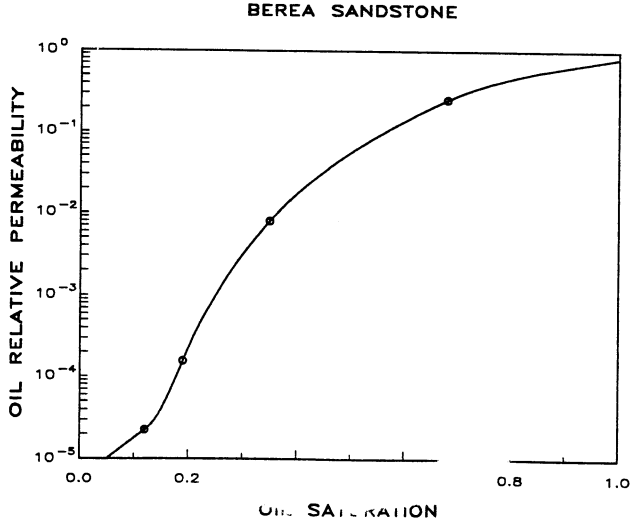

Fig.12—Estimated Oil Relative Permeability Curve Using Procedure I

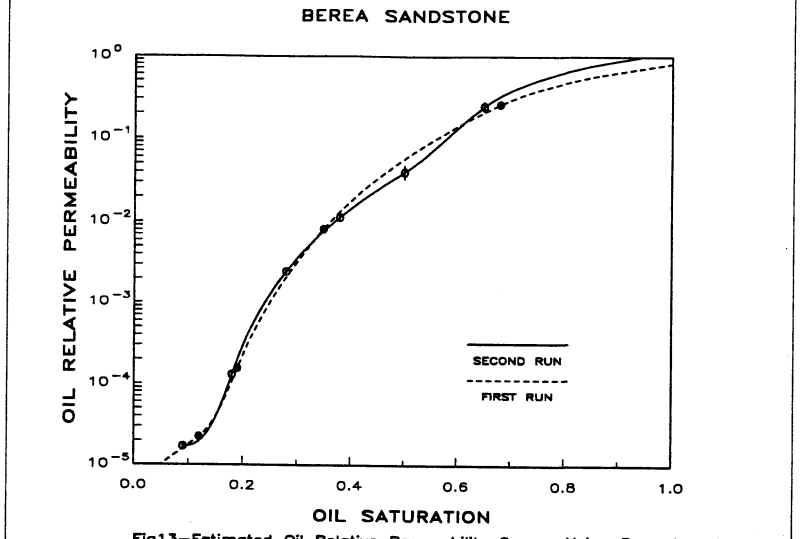

Fig13—Estimated Oil Relative Permeability Curves Using Procedure I

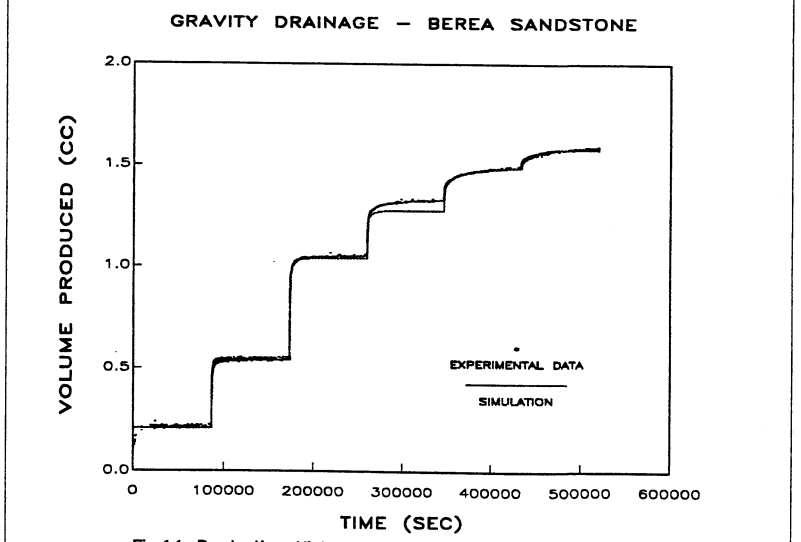

Fig.14—Production History and History Match Using Procedure II

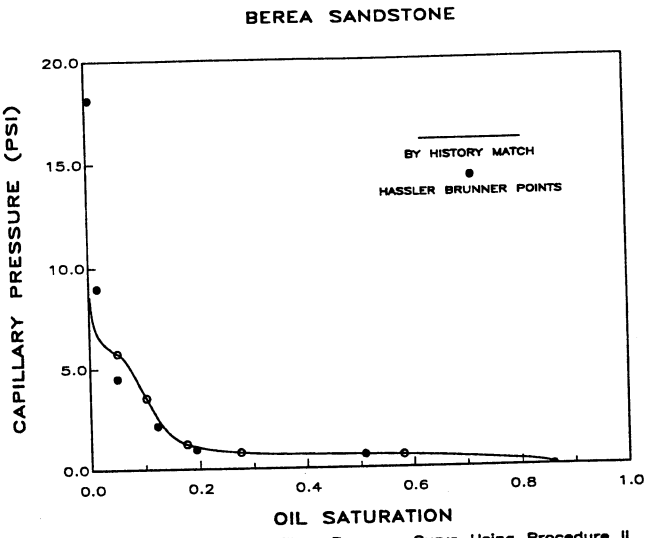

Fig.15—Estimated Capillary Pressure Curve Using Procedure II

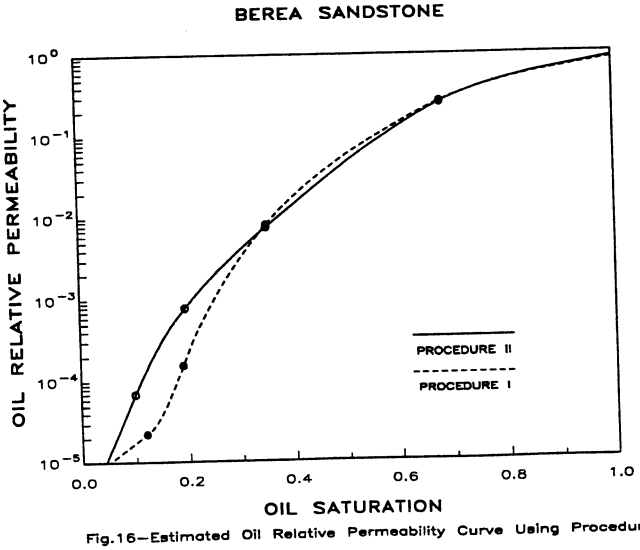

Fig.16—Estimated Oil Relative Permeability Curve Using Procedure II